# Numerical representation of internal waves propagation

Jérémie Demange, Laurent Debreu, Patrick Marchesiello, Florian Lemarié, Eric Blayo


# Numerical representation of internal waves propagation

J. Demange, L. Debreu, P. Marchesiello, F. Lemarié, E. Blayo

RESEARCH REPORT
N° 8590
August 2014
Project-Team MOISE

ISSN 0249-6399 ISRN INRIA/RR--8590--FR+ENG

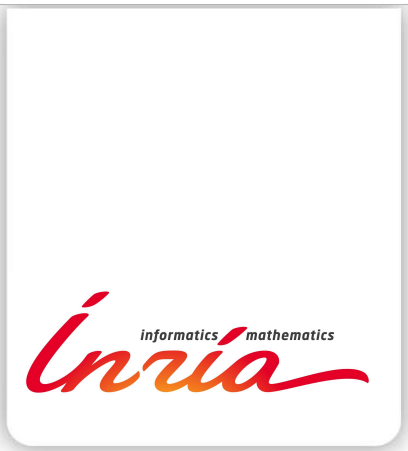


# Numerical representation of internal waves propagation

J. Demange, L. Debreu, P. Marchesiello, F. Lemarié, E. Blayo

Project-Team MOISE

Research Report n° 8590 — August 2014 — 21 pages

**Abstract:** Similar to surface waves propagating at the interface of two fluid of different densities (like air and water), internal waves in the oceanic interior travel along surfaces separating waters of different densities (e.g. at the thermocline). Due to their key role in the global distribution of (physical) diapycnal mixing and mass transport, proper representation of internal wave dynamics in numerical models should be considered a priority since global climate models are now configured with increasingly higher horizontal/vertical resolution. However, in most state-of-the-art oceanic models, important terms involved in the propagation of internal waves (namely the horizontal pressure gradient and horizontal divergence in the continuity equation) are generally discretized using very basic numerics (i.e. second-order approximations) in space and time. In this paper, we investigate the benefits of higher-order approximations in terms of the discrete dispersion relation (in the linear theory) on staggered and nonstaggered computational grids. A fourth-order scheme discretized on a C-grid to approximate both pressure gradient and horizontal divergence terms provides clear improvements but, unlike nonstaggered grids, prevents the use of monotonic or non-oscillatory schemes. Since our study suggests that better numerics is required, second and fourth order direct space-time algorithms are designed, thus paving the way toward the use of efficient high-order discretizations of internal gravity waves in oceanic models, while maintaining good stability properties (those schemes are stable for Courant numbers smaller than 1). Finally, important results obtained at a theoretical level are illustrated at a discrete level using two-dimensional ($x$,$z$) idealized experiments.

**Key-words:** Internal gravity waves, Grid staggering, Direct space time algorithms

**RESEARCH CENTRE**
**GRENOBLE – RHÔNE-ALPES**

Inovallée
655 avenue de l'Europe Montbonnot
38334 Saint Ismier Cedex

# Représentation numérique de la propagation des ondes internes

**Résumé :** De manière analogue aux ondes de surface se propageant à l'interface entre deux fluides de densité différente (tels que l'air et l'eau), les ondes internes dans l'océan intérieur se propagent le long des surfaces séparant des masses d'eau de différentes densités (e.g. au niveau de la thermocline). Du fait de leur rôle clé dans la distribution globale du mélange diapycnal et du transport de masses d'eau, la bonne représentation de la dynamique des ondes internes dans les modèles numérique doit devenir une priorité car les modèles globaux de climat sont maintenant intégrés à des résolutions permettant de marginalement la résoudre. Cependant, dans la plupart des modèles d'océan, les termes importants intervenant dans la propagation des ondes internes (à savoir le gradient de pression horizontal et le calcul de divergence dans l'équation de continuité) sont généralement discrétisés avec des schémas d'ordre peu élevé en espace et en temps (typiquement à l'ordre 2). Dans ce papier, nous illustrons les bénéfices d'une augmentation de la précision pour différents arrangements des variables sur la grille de calcul (i.e. grilles décalées ou colocalisées) en se basant sur la relation de dispersion au niveau discret (dans le cas linéaire). L'utilisation d'un schéma centré d'ordre 4 sur grille C pour approcher les termes de gradient de pression et de divergence horizontale apporte des améliorations significatives mais, à l'inverse des grilles colocalisées, ne permet pas l'utilisation de schémas monotones ou non-oscillants. Notre étude suggère qu'une amélioration des schémas numériques est nécessaire, nous proposons donc le développement de schémas couplés espace-temps spécifiquement destinés à l'intégration des ondes internes. Des schémas d'ordre 2 et 4 sont mis au point, ceux-ci allient de bonnes propriétés de précision et de stabilité (ils sont stables pour des nombres de Courant inférieurs à 1). Finalement, les résultats obtenus au niveau théorique sont illustrés au niveau discret à l'aide d'expériences effectuées dans un cadre semi-idéalisé.

**Mots-clés :** Ondes internes de gravité, Arrangement des variables, Schémas couplés espace-temps

# 1 Introduction

Internal waves are ubiquitous in the oceanic interior and have received much attention by oceanographers due to the pivotal role of internal-wave driven mixing in maintaining the ocean stratification and meridional overturning circulation. Internal waves can arise in a variety of ways, by the action of atmospheric fronts, tides, wind-stress, current-topography interactions, etc. Numerous studies have been dedicated to a better understanding of internal waves generation, propagation, dissipation, and their role on Earth's climate, either from observations or numerical simulations. In a numerical model, proper representation of internal waves dynamics is directly linked to horizontal and vertical resolution, but also to the numerical schemes used to discretize horizontal pressure gradient and horizontal divergence in the continuity equation.

Most oceanic numerical models employ low-order space-time discretization schemes to integrate internal waves dynamics. This choice has been historically made to offer the best efficiency factor (i.e. the CFL number divided by the number of evaluation of the right hand side) with less emphasis on accuracy. Indeed, for low-resolution global climate models, most of the internal wave spectrum is not resolved, hence the numerical algorithms were only chosen to maintain good stability properties (e.g. [3]). However, thanks to advances in computational power, global climate models are now configured with increasingly higher horizontal/vertical resolution (it must be clear that both horizontal and vertical wavenumbers are involved in the dispersion relation). Since the typical grid-spacing in the new generation of global models is around $1/10^\circ$ (at midlatitudes), a wide part of the internal waves spectrum could be potentially represented by the corresponding computational grid. It is, thus, legitimate to reassess the historical numerical choices for the space-time integration of internal gravity waves. In particular, current low-order schemes are prone to dispersion errors and may then induce erroneous energy transfers through nonlinearities and aliasing [9].

The objective of this paper is to check numerical schemes against the linear theory for which the characteristics of internal waves are well known. Many studies have emphasized the role of the grid staggering (cf. figure 1) for the proper representation of internal and external inertia-gravity waves [12, 14]. More specifically, internal gravity waves representation can be studied using the following system of equations

$$\begin{aligned} \frac{\partial u}{\partial t} - f\,v + g\frac{\partial h}{\partial x} &= 0 \\ \frac{\partial v}{\partial t} + f\,u + g\frac{\partial h}{\partial y} &= 0 \\ \frac{\partial h}{\partial t} + H\left(\frac{\partial u}{\partial x} + \frac{\partial v}{\partial y}\right) &= 0 \end{aligned} \tag{1}$$

where $u$,$v$ are the horizontal velocity components, $f$ is the Coriolis parameter, $H$ the constant water depth and $h$ the displacement. To solve (1), the criteria to discriminate the available choice of computational grids (structured or unstructured) and staggerings are

- the treatment of the Coriolis force
- the proper representation of Rossby waves
- the computation of the pressure gradient term

Nowadays, the Arakawa $C$-grid is the preferred staggering for high resolution simulations because it is assumed that the computational mode in the averaging of the Coriolis force is controlled by viscous or diffusive terms. On the contrary, the Arakawa $B$-grid should remain the preferred

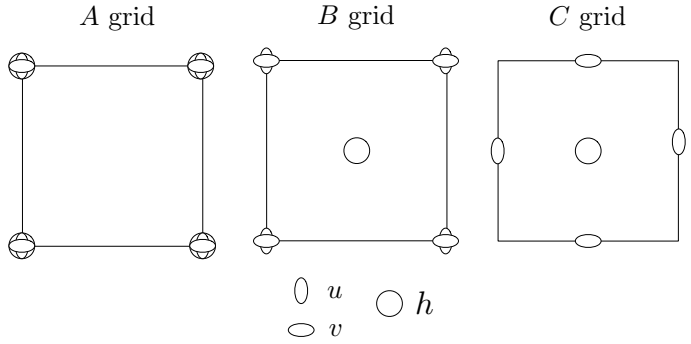


Figure 1: Arakawa $A$, $B$ and $C$-grids

approach for coarse resolution models because it allows a natural discretization of the Coriolis term without averaging. The $A$-grid has the same advantage but requires averaging to compute the pressure gradient term and the continuity equation. For structured grids, most comparisons between $A$, $B$ and $C$-grids have been done using low order (second order) schemes. In this paper, we first show that higher order schemes show clear improvements whatever the grid staggering. For internal waves, the discretization order is directly linked to the order of approximation of both the pressure gradient term and of the horizontal divergence term of the continuity equation.

In the following, we neglect the Coriolis term and focus on the pressure gradient term in the 2D $(x, z)$ framework. In this $(x,z)$ case, the $C$-grid will be referred to as the *staggered grid* and the $A$-grid to as the *non staggered grid*. The $A$-grid (like the $B$-grid in 3D) is prone to a computational mode when computing the pressure gradient term. This problem has been extensively studied in several papers in the shallow water case both for structured and unstructured grids [19]. In the shallow-water case, a solution is to add a velocity-dependent dissipation (e.g. using a discontinuous Galerkin method) in order to introduce enough damping of the computational mode. In the 3D case, in the presence of internal gravity waves, this is more difficult to handle since this diffusion term should be proportional to the speed of internal gravity waves which are usually not explicitly computed (indeed, it would require the solution of a boundary value problem every time-step at each grid point). Here we propose to compute these phase speeds via a vertical normal mode decomposition, thus enabling an efficient damping of the computational mode without affecting the main signal. The computation of these speeds also enables the setup of direct space-time algorithms. It thus opens the path toward fully space time algorithms for numerical ocean models.

The paper is organized as follows. Section (2) contains a brief remainder of the normal mode decomposition and the derivation of internal gravity waves characteristics. Section (3) recalls the usual discretization properties, with a focus on higher-order approximations of the pressure gradient term and horizontal divergence, both on unstaggered and staggered grids. We also introduce an internal wave speed dependent dissipation for the damping of the computational mode on the non staggered grids. In section (4), idealized numerical experiments illustrate the theoretical results obtained in section (3). In the last section, we focus on the derivation of direct space time algorithms both on unstaggered and staggered grids, resulting in highly efficient algorithms for the numerical propagation of internal gravity waves. These schemes are also reliable for integration of external gravity waves of the barotropic part of a 3D ocean model (where the propagation speed is know in advance). Conclusions and perspectives are then drawn.

## 2 Normal mode decomposition

In this section, we briefly summarize salient points regarding the normal mode decomposition of the 2D ($x$-$z$) linearized (around $u = u_0$) flat bottom inviscid primitive equations (i.e. under the hydrostatic and Boussinesq assumptions). See [13, 8, 11] for more details about the vertical mode decomposition. In the following, $u(x, z, t)$ and $w(x, z, t)$ denote the perturbation components of fluid velocities, $p(x, z, t)$ and $\rho(x, z, t)$ denote pressure and density perturbations around a state $(\bar{p}(z), \bar{\rho}(z))$ satisfying the hydrostatic balance $\dfrac{\mathrm{d}\bar{p}(z)}{\mathrm{d}z} = -\bar{\rho}(z)g$ where $\overline{\rho}(z)$ is a reference density profile. Using those notations, the system of interest reads

$$\frac{\partial u}{\partial t} + u_0\frac{\partial u}{\partial x} + \frac{1}{\rho_0}\frac{\partial p}{\partial x} = 0 \qquad \text{Momentum conservation} \tag{2}$$

$$\frac{\partial p}{\partial z} = -g\rho \qquad \text{Hydrostatic equilibrium} \tag{3}$$

$$\frac{\partial u}{\partial x} + \frac{\partial w}{\partial z} = 0 \qquad \text{Continuity / Incompressibility} \tag{4}$$

$$\frac{\partial \rho}{\partial t} + u_0\frac{\partial \rho}{\partial x} + w\frac{\mathrm{d}\overline{\rho}}{\mathrm{d}z} = 0 \qquad \text{Energy conservation} \tag{5}$$

In the vertical direction the model extends from the flat bottom $z = -H$ to the free surface $z = \eta(x, t)$. Since we are interested in internal gravity waves dynamics we assume a rigid lid i.e. $\dfrac{\partial \eta}{\partial t} = 0$[1]. Under this assumption, the surface and bottom boundary conditions read

$$\frac{\partial \eta}{\partial t} = 0 \tag{6}$$

$$w(z = -H) = 0 \tag{7}$$

On a discrete grid, with $n$ vertical levels, the solutions of (2,3,4,5) can be decomposed using vertical modes $M_q(z)$:

$$\begin{cases} u(x,z,t) = \displaystyle\sum_{q=0}^{n-1} u_q(x,t)M_q(z) \\ p(x,z,t) = \rho_0 g \displaystyle\sum_{q=0}^{n-1} h_q(x,t)M_q(z) \\ \rho(x,z,t) = -\rho_0 \displaystyle\sum_{q=0}^{n-1} h_q(x,t)\frac{\mathrm{d}M_q(z)}{\mathrm{d}z} \end{cases} \tag{8}$$

where the modes $M_q(z)$ are the eigenvectors of the following Sturm-Liouville problem[2]

$$\begin{cases} \Lambda M_q = \lambda_q M_q \\ \partial_z M_q|_0 = 0 \\ \partial_z M_q|_{-H} = 0 \end{cases} \tag{9}$$

[1] This rigid lid assumption classically leads to a surface pressure that is diagnosed in order to get a non divergent depth integrated flow.

[2] note that because of the rigid-lid assumption the top boundary condition for the Sturm-Liouville problem (9) is no longer $\left.\dfrac{\mathrm{d}M_q}{\mathrm{d}z}\right|_{z=0} = -\dfrac{N^2(0)}{g}M_q(0)$ as in [8, 11], but simply $\left.\dfrac{\mathrm{d}M_q}{\mathrm{d}z}\right|_{z=0} = 0$

where $\Lambda = -\dfrac{\mathrm{d}}{\mathrm{d}z}\left(N^{-2}\dfrac{\mathrm{d}}{\mathrm{d}z}\right)$, with $N^2(z) = -\dfrac{g}{\rho_0}\dfrac{\mathrm{d}\overline{\rho}}{\mathrm{d}z}$ the Brünt-Vaisala frequency assumed to be positive. Each mode $M_q(z)$ is associated to a positive eigenvalue $\lambda_q = c_q^{-2}$ (sorted in increasing order). The vertical modes are orthonormal with respect to the dot product $\langle f, g\rangle = \dfrac{1}{H}\displaystyle\int_{-H}^{0} f(z)g(z)dz$. The first mode ($q = 0$) is called the barotropic mode and is depth-independent (i.e. $\lambda_0 = 0$) under the rigid lid assumption. For constant $N$, an analytical expression of the modes and their associated eigenvalues can easily be found [5]

$$M_q(z) = \sqrt{2}\cos\left(\frac{q\pi}{H}z\right), \qquad c_q = \frac{NH}{q\pi}, \qquad q \geq 1 \tag{10}$$

Figure (2) shows the first four baroclinic modes for $H = 4000$m and $N = 2.10^{-3}\mathrm{s}^{-1}$. Projection

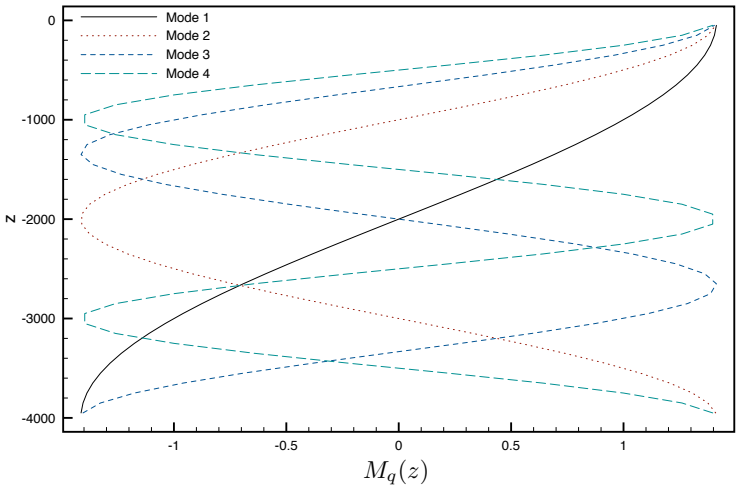


Figure 2: Baroclinic modes $M_q(z)$ (defined in (10)) for $1 \leq q \leq 4$ with respect to the depth $z$.

of equations (2,3,4,5) onto the vertical modes $M_q$ leads to the following system for $q \geq 1$ :

$$\partial_t u_q + u_0\frac{\partial u_q}{\partial x} + g\partial_x h_q = 0 \tag{11}$$

$$\partial_t h_q + u_0\frac{\partial h_q}{\partial x} + \frac{c_q^2}{g}\partial_x u_q = 0 \tag{12}$$

At this point, let us draw two important remarks

- (11) is obtained by multiplying the momentum equation (2) by $M_q$ and integrating over $[-H, 0]$. The order of accuracy for the discretization of $\partial_x h_q$ is thus directly linked to the order of accuracy of the pressure gradient discretization.

- (12) is obtained by multiplying the density equation (5) by $N^{-2}(z)\dfrac{\mathrm{d}M_q}{\mathrm{d}z}$, integrating over $[-H, 0]$ and using the continuity equation. The order of accuracy for the discretization of the term $\partial_x u_q$ is linked to the order of approximation of the horizontal divergence in the continuity equation.

As mentioned earlier, the pressure gradient term and the divergence in the continuity equation are generally discretized using low-order (second-order) approximations.

In (11-12), each modal projection leads to a shallow water system which can also be expressed in terms of characteristic variables. The corresponding characteristic variables $y_q$ are

$$y_q^{\pm} = u_q \pm \frac{g}{c_q} h_q$$

which propagate at speed $u_0 \pm c_q$, they indeed satisfy the transport equation

$$\frac{\partial y_q^{\pm}}{\partial t} + (u_0 \pm c_q)\frac{\partial y_q}{\partial x} = 0 \tag{13}$$

In practice, internal waves can be forced by barotropic tides at a given frequency $\omega$, so that the wavenumber associated to the baroclinic mode $q$ is given by

$$k_q = \frac{\omega}{c_q}$$

The main objective of this paper is to look at the numerical accuracy of the discrete propagation of these internal waves in an ocean model.

# 3 Discretization of internal waves in ocean models

## 3.1 Accuracy and grid staggering

In most ocean models, the approximation of (11,12) is done with second-order accuracy (in space and time). Indeed, both horizontal pressure gradient and horizontal divergence are computed at second order. Numerical models are generally discretized on a grid where velocity and pressure are staggered (Arakawa $C$-grid in the horizontal). The $C$-grid is superior to the non staggered $A$-grid at high resolution whereas the non staggered grid is advantageous for the computation of the Coriolis term, prominent at low resolution [15]. In the following, we consider only the pressure gradient term in a 2D $x$-$z$ domain without rotation so that this problem is absent. However, we keep in mind that staggered grids are not fundamentally better especially for applications at medium and coarse resolution (e.g. climate simulations).

Let us rewrite baroclinic mode $q$ around a state at rest ($u_0 = 0$):

$$\begin{cases} \dfrac{\partial u_q}{\partial t} + g\dfrac{\partial h_q}{\partial x} = 0 \\ \dfrac{\partial h_q}{\partial t} + \dfrac{c_q^2}{g}\dfrac{\partial u_q}{\partial x} = 0 \end{cases}$$

As mentioned earlier, we consider two staggerings : a first one analogous to A-GRID and a second one analogous to a C-GRID in 2D. The corresponding variable arrangement is represented in figure (3). Assuming that the space increment $\Delta x$ is constant, the second and fourth order approximation of spatial derivatives on the $A$- and $C$-grids are

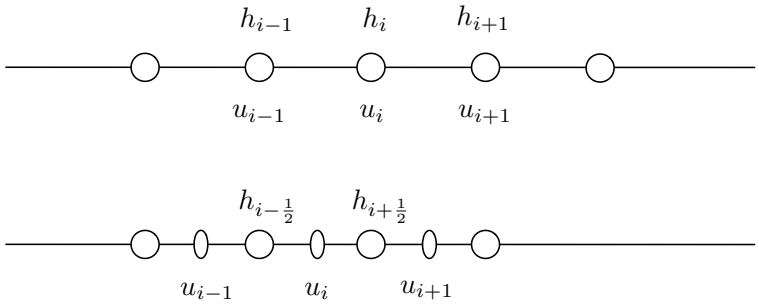


Figure 3: Grid staggering : A grid (top), C grid (bottom)

$$
\begin{aligned}
A\text{-GRID:} \quad \left.\frac{\partial f(x)}{\partial x}\right|_{2^{\text{nd}}\text{order}} &= \frac{1}{2\Delta x}\left(f(x+\Delta x)-f(x-\Delta x)\right)+\mathcal{O}(\Delta x)^2 \\
\left.\frac{\partial f(x)}{\partial x}\right|_{4^{\text{th}}\text{order}} &= \frac{1}{2\Delta x}\left(f(x+\Delta x)-f(x-\Delta x)\right) \\
&\quad -\frac{1}{12\Delta x}\left(f(x+2\Delta x)-2f(x+\Delta x)+2f(x-\Delta x)-f(x-2\Delta x)\right)+\mathcal{O}(\Delta x)^4 \\
C\text{-GRID:} \quad \left.\frac{\partial f(x)}{\partial x}\right|_{2^{\text{nd}}\text{order}} &= \frac{1}{\Delta x}\left(f(x+\Delta x/2)-f(x-\Delta x/2)\right)+\mathcal{O}(\Delta x)^2 \\
\left.\frac{\partial f(x)}{\partial x}\right|_{4^{\text{th}}\text{order}} &= \frac{1}{\Delta x}\left(f(x+\Delta x/2)-f(x-\Delta x/2)\right) \\
&\quad -\frac{1}{24\Delta x}\left(f(x+3\Delta x/2)-3f(x+\Delta x/2)+3f(x-\Delta x/2)-f(x-3\Delta x/2)\right)+\mathcal{O}(\Delta x)^4
\end{aligned}
$$

The exact phase velocity is given by $v_q^{\text{exact}} = \dfrac{\omega^{\text{exact}}}{k} = c_q$ while the numerical phase velocity is given by $v_q^{\text{num}} = \dfrac{\omega^{\text{num}}}{k}$. A simple Fourier analysis (see [16]) gives the numerical phase error $v^{\text{num}}/v^{\text{exact}}$ indicated in table (1) as a function of the normalized wavenumber $k\Delta x$. The cor-

| | $A$-Grid | $C$-Grid |
|---|---|---|
| C2 (centered second order ) | $\dfrac{\sin k\Delta x}{k\Delta x}$ | $\dfrac{\sin k\Delta x/2}{k\Delta x/2}$ |
| C4 (centered fourth order ) | $\dfrac{(4-\cos k\Delta x)\sin k\Delta x}{3k\Delta x}$ | $\dfrac{(13-\cos k\Delta x)\sin k\Delta x/2}{6k\Delta x}$ |

Table 1: Numerical phase error for centered second and fourth order approximations on the $A$ and $C$-grids

responding phase errors are plotted in figure (4). As expected, higher order discretization of horizontal pressure gradient and horizontal divergence naturally lead to a better propagation of internal gravity waves. Indeed, we see that the phase error is significantly reduced when going from a second-order to a fourth-order approximation of $\partial_x h_q$ and $\partial_x u_q$ in (11-12), whatever the grid-staggering. In particular for the $C$-grid the improvement is over the whole wave spectrum while for the $A$ grid the $2\Delta x$ wave remains unchanged (computational mode). On the $A$-grid, the

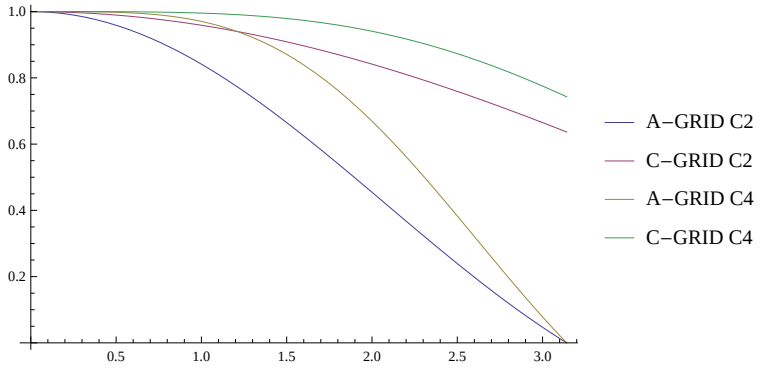


Figure 4: Phase error with respect to the wavenumber $k\Delta x$ for $A$ and $C$ grid for second and fourth order approximations

error reduction is significant on a large part of the wave spectrum. The computational mode on the $A$-grid justifies the need for additional numerical diffusion which is the subject of subsection (3.2). This is less needed for the $C$-grid because all scales are well resolved, especially when using a fourth-order approximation.

**Practical implementation of the fourth order discretizations** As previously mentioned, better accuracy in the propagation of internal waves requires more accurate approximations of both the horizontal pressure gradient and the continuity equation. Both components have to be computed at high order since their role is equally important. The horizontal divergence should thus be computed using fourth order approximation and the result is used to deduce the vertical velocity from the continuity equation (4). Note that this high order computation of the horizontal divergence is also more in agreement with what is done in some numerical ocean models (e.g. NEMO, ROMS) for the nonlinear advection term (not present in our linear equations) : the velocity at mid points is computed using fourth order interpolation. In this case, using only a second order approximation in the continuity equation, introduces a problem of *constancy preservation* of momentum in a way identical to the constancy preservation for tracers [10].

## 3.2 Damping of the numerical mode of the nonstagerred grids

Let us note $A_h, A_v$ the horizontal/vertical viscosity coefficients and $K_h, K_v$ the horizontal/vertical diffusion coefficients. We allow the possibility for the $A_h, A_v, K_h, K_v$ coefficients to be constant or dependent on the grid size and local velocity to represent second order implicit diffusion associated to odd-ordered advection schemes/time integration scheme. For vertical diffusion, we assume a simple parameterization based on the Brunt-Vaisala frequency [17] which will enable us to project the equations onto the vertical modes, as follows

$$\left\{ \begin{array}{l} \dfrac{\partial u}{\partial t} + u_0 \dfrac{\partial u}{\partial x} + \dfrac{1}{\rho_0} \dfrac{\partial p}{\partial x} = A_h \dfrac{\partial^2 u}{\partial x^2} + \dfrac{\partial}{\partial z} \left( A_v N^{-2}(z) \dfrac{\partial u}{\partial z} \right) \\ \dfrac{\partial \rho}{\partial t} + u_0 \dfrac{\partial \rho}{\partial x} + w \dfrac{\partial \overline{\rho}}{\partial z} = K_h \dfrac{\partial^2 \rho}{\partial x^2} + \dfrac{\partial}{\partial z} \left( K_v N^{-2}(z) \dfrac{\partial \rho}{\partial z} \right) \end{array} \right. \tag{14}$$

Using (8,9) we obtain

$$\begin{cases} \dfrac{\partial u_q}{\partial t} + u_0 \dfrac{\partial u_q}{\partial x} + g \dfrac{\partial h_q}{\partial x} = A_h \dfrac{\partial^2 u_q}{\partial x^2} - \lambda_q A_v u_q \\ \dfrac{\partial h_q}{\partial t} + u_0 \dfrac{\partial h_q}{\partial x} + \dfrac{c_q^2}{g} \dfrac{\partial u_q}{\partial x} = K_h \dfrac{\partial^2 h_q}{\partial x^2} - \lambda_q K_v h_q \end{cases}$$

which in term of characteristic variables $y_q^{\pm} = u_q \pm \dfrac{g}{c_q} h_q$ leads to

$$\begin{aligned} \frac{\partial y_q^+}{\partial t} + (u_0 + c_q) \frac{\partial y_q^+}{\partial x} &= \alpha_h \frac{\partial^2 y_q^+}{\partial x^2} + \beta_h \frac{\partial^2 y_q^-}{\partial x^2} - \lambda_q \alpha_v y_q^+ - \lambda_q \beta_v y_q^- \\ \frac{\partial y_q^-}{\partial t} + (u_0 - c_q) \frac{\partial y_q^-}{\partial x} &= \alpha_h \frac{\partial^2 y_q^-}{\partial x^2} + \beta_h \frac{\partial^2 y_q^+}{\partial x^2} - \lambda_q \alpha_v y_q^- - \lambda_q \beta_v y_q^+ \end{aligned} \tag{15}$$

where

$$\alpha_h = \frac{1}{2}\left(A_h + K_h\right), \beta_h = \frac{1}{2}\left(A_h - K_h\right), \quad \alpha_v = \frac{1}{2}\left(A_v + K_v\right), \beta_v = \frac{1}{2}\left(A_v - K_v\right)$$

From (15) we can draw a few Comments:

1. We can notice that if the numerical Prandlt number $\dfrac{A_h}{K_h}$ is not equal to one (i.e. for $\beta_h \neq 0$), the two characteristics are mixed together. The same holds for vertical viscosities/diffusivities ($\beta_v \neq 0$). More generally if different advection schemes (diffusive or not) are used for density and momentum, we expect the two characteristics to become dependent one to the other in contradiction with the theory.

2. In terms of characteristics variables, Horizontal diffusion (through $A_h$, $K_h$) induces a diffusion coefficient which is independent of the propagation speed[3]. The exact dispersion relation for the characteristic variables is $\omega_q^{\pm} = \pm k c_q$. With $A_v, K_v = 0$, the dispersion relation associated to (15) is

   $$\omega_q^{\pm} = \pm k \sqrt{c_q^2 - \beta_h^2 k^2} - i \alpha_h k_q^2$$

   For small values of $\beta_h$ such that $\beta_h^2 k^2 \leq c_q^2$ we get

   $$\omega_q^{\pm} = \pm k c_q \sqrt{1 - \left(\frac{\beta_h k}{c_q}\right)^2} - i \alpha_h k_q^2$$

   which shows dispersion errors, while for larger values such that $\beta_h^2 k^2 \geq c_q^2$, it leads to purely imaginary frequency

   $$\omega_q^{\pm} = -i \left[ \pm k_q c_q \sqrt{\left(\frac{\beta_h k}{c_q}\right)^2 - 1} + \alpha_h k_q^2 \right]$$

   Previous relations show that if the difference between horizontal viscosity and diffusivity is too large, some of the internal waves will stop propagating.

[3] This is not true however if $A_h$ comes from a diffusive time stepping. As an example, a first order dissipative forward backward scheme will lead to a coefficient $A_h$ proportional to $c_q^2$.

3. When projected onto the characteristic variables, vertical diffusion based on the Brunt-Vaisala frequency results in a friction term with a coefficient dependent on the internal wave speed (the $\lambda_q \beta_v y_q^{\pm}$ terms in (15) ). The coefficient behaves like $\frac{1}{c_q^2}$, it is therefore larger for high baroclinic modes. Moreover, this friction term is not a scale selective filter.

**Diffusion based on internal waves phase speed** The vertical mode decomposition (15) allows to compute an internal wave speed dependent diffusion. Since we are mainly interested in the amount of diffusion necessary to properly integrate internal waves, the idea is not to formulate the numerical model entirely in terms of the vertical modes (e.g. [7]). Indeed, from our perspective, the projection onto the vertical modes will be done only to compute the diffusive term. This diffusive term will be then expressed back in terms of primitive variables. Any dissipative numerical scheme can be used for the propagation of internal gravity waves, like (high order) upwind schemes or monotone advection schemes. However, this choice has to be done carefully for the following reasons:

- The use of first order upwind schemes (whose diffusion coefficients, associated to the leading term in the truncation error, equal $\frac{1}{2} c_q \Delta x$) would lead to a too diffusive solution. But the vertical mode decomposition offers the possibility to build high order non oscillatory schemes acting directly on the characteristic variables that take into account the local regularity of the discrete solution. The design of non oscillatory schemes may also be required in case of internal waves breaking behaving like hydraulic jumps.
- The numerical advection schemes when formulated in terms of characteristic variables take into account the direction of propagation. This makes the problem of open boundary conditions specification well posed ([8]) with respect to internal waves.
- There are fundamental differences between formulation (15) based on characteristic variables and the traditional formulation (14) based on primitive variables. In the diffusion based on characteristic variables, an irregularity in the density field is immediately "felt" by momentum through the added diffusion (and vice versa). This is not the case when the diffusive term are put independently on momentum and tracers, as in (14).

# 4 Numerical experiment

In this section, we use idealized numerical experiments to look first at the impact of increasing the order of the discrete approximations of the pressure gradient and horizontal divergence terms (both on $A$ and $C$-grid), and secondly at the use of internal wave phase speed dependent diffusion coefficients.

## 4.1 Design of the numerical test

The domain is a vertical section with $L_x = 2000$km and $H = 4$km. The initial condition is given in term of modal decomposition and corresponds to right travelling only waves (i.e. $y_q^- = u_q - \frac{g}{c_q} h_q = 0$):

$$\text{For } 1 \leq n \leq n_{\max}, \quad h_n(x, t=0) = \frac{1}{n} \cos(k_n x) e^{-(x-x_0)^2/\sigma^2}, \qquad u_n(x, t=0) = \frac{g}{c_n} h_n(x, t=0) \tag{16}$$

where $k_n = \dfrac{\omega}{c_n}$, $\omega = \omega_{M2} = 1,405.10^{-4}\text{s}^{-1}$ (corresponding to the M2 barotropic tide), $x_0 = L/5$, $\sigma^2 = 6000L_x$. The Brunt-Vaisala Frequency is constant and set to $N = 2.10^{-3}\text{s}^{-1}$. Each mode has wavelength $\lambda_n = 2\pi/k_n = 2\pi c_n/\omega$. Let $n_{\max}$ be the number of modes, the smallest wavelength is given by $\lambda_{\min} = \lambda_{n_{\max}} = 2\pi c_{n_{\max}}/\omega$.
In the case of constant $N$, we have

$$\lambda_{\min} = \frac{2\pi NH}{n_{\max}\pi\omega} = \frac{2NH}{n_{\max}\omega}$$

So that if we want the initial wave to be resolved by the grid we have to choose $n_{\max}$ such that $\lambda_{\min} \geq 2\Delta x$ which leads to

$$n_{\max} \leq \frac{NH}{\omega\Delta x} \tag{17}$$

In the numerical experiments, we will use $\Delta x = 4$km and $\Delta x = 2$km. Using (17) for the coarsest resolution case $\Delta x = 4$km we get

$$n_{\max} \leq \frac{2.10^{-3}10^4}{1,405.10^{-4}10^4} \approx 14.3$$

In (16), $n_{\max}$ is fixed to 14. The corresponding initial condition is plotted in figure (5).

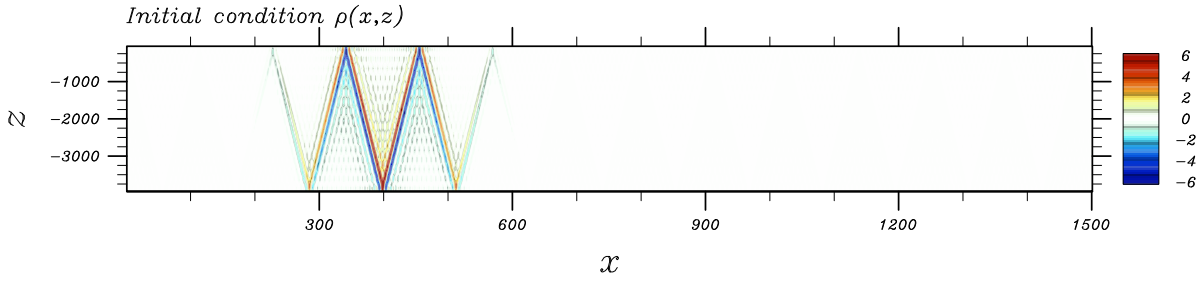


Figure 5: Density field : initial condition

The time integration is done using a fourth-order Runge-Kutta method (referred to as RK4) to match the order of accuracy in space.

## 4.2 Low vs high order discretization of internal waves

In this first series of experiments, we investigate the impact of going from a second order (C2) scheme to a fourth order (C4) scheme to discretize both horizontal pressure gradient and horizontal divergence in the continuity equation. The impact of grid staggering is also investigated. Figures (6, 7) show the solutions at final time for the $\Delta x = 4$km and $\Delta x = 2$km resolution. Vertical lines are added to more easily see the dispersion error in comparison with the analytical solution. The corresponding relative RMS errors are indicated on figure (8). These simulations is constant with the theoretical dispersive errors given in figure (4). Figures (6, 7) show that fourth-order accuracy leads to a significant improvement for the $A$-grid at large scales. Concerning the $C$-grid the improvement is over the whole spectrum, as seen in figure (8) the resulting RMS error at high resolution ($\Delta x = 2$km) is much lower than the one obtained with second order

schemes. This favors the use of the staggered grid. However we remind the computational mode associated with the treatment of the Coriolis term in the horizontal with this kind of staggering. Moreover, in these configurations, only the $A$-grid allows the design of monotone schemes for internal-gravity waves propagation since the velocity and density are collocated so that the discrete definition of the characteristic variables, which combine these two fields, is straightforward and does not require any averaging.

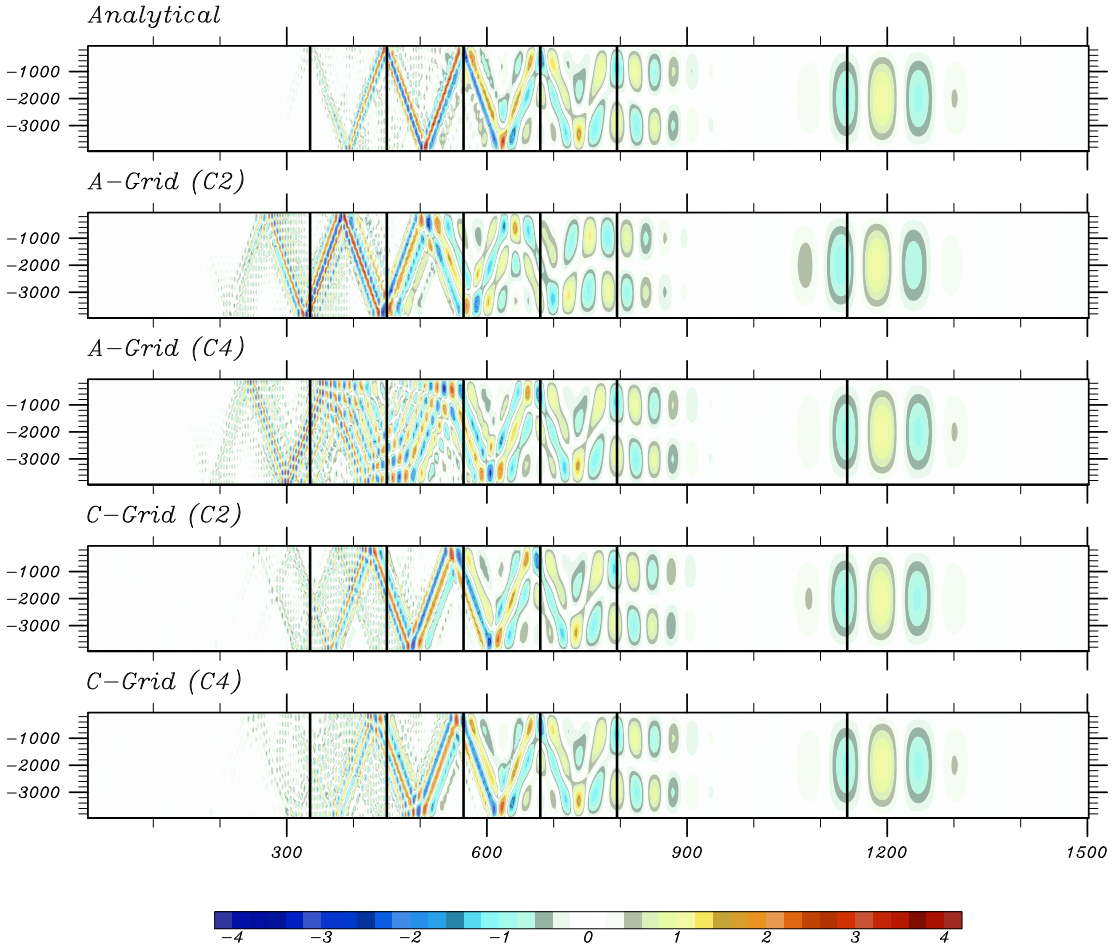


Figure 6: Comparison of second (C2) and fourth (C4) order centered schemes against the analytical solution for the $A$ and $C$-grid. Density field for $\Delta x = 4$km

## 4.3 Diffusion scaled on internal wave phase speed

The preceding results clearly show the emergence of a numerical mode on the non staggered $A$-grid. The objective, here, is to add diffusion based on the internal wave phase speed to damp this computational mode. To be able to compare with the fourth order centered scheme, we have implemented a fourth order scheme with total variation diminishing (TVD) limiters. The limiters used in these simulations correspond to the minimum of the TVD region ([16]). This

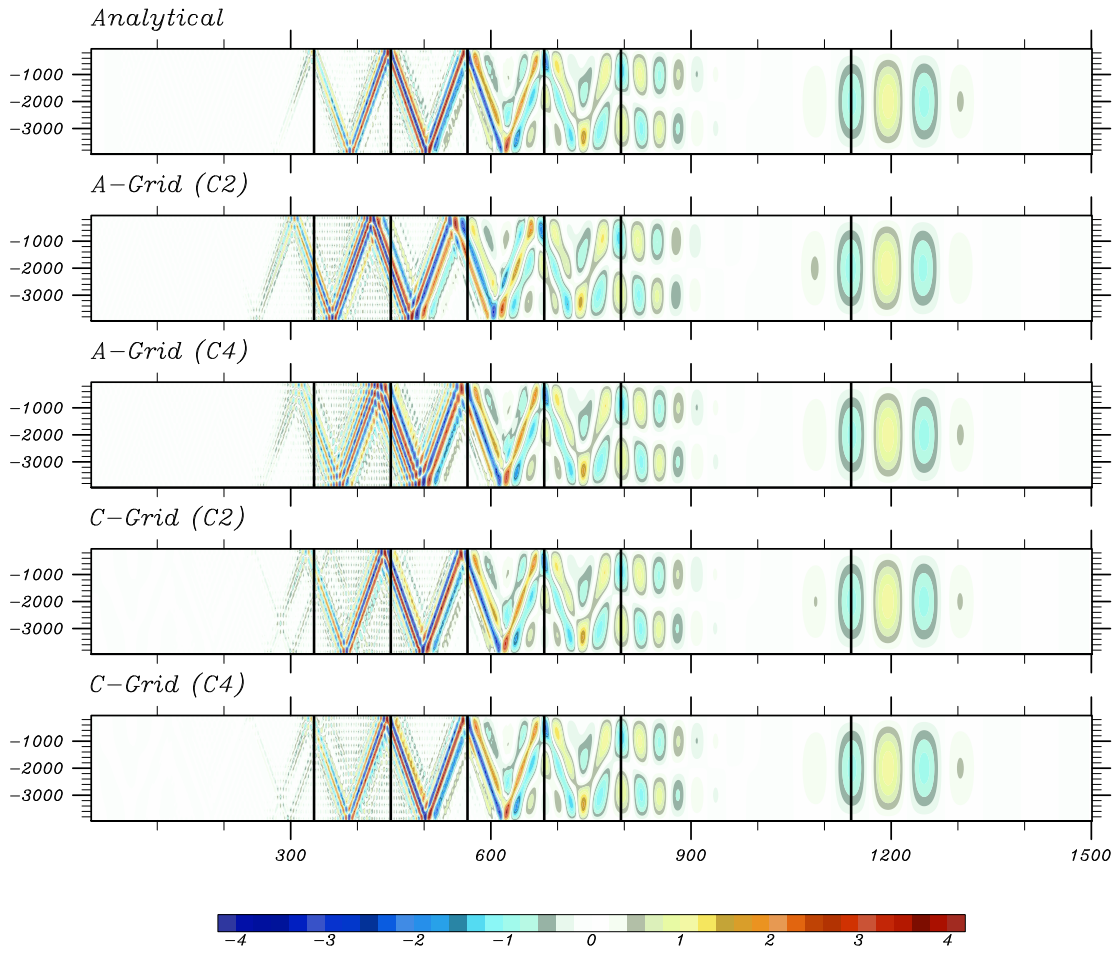


Figure 7: Comparison of second (C2) and fourth (C4) order centered schemes against the analytical solution for the $A$ and $C$-grid. Density field for $\Delta x = 2$km

naturally induces a velocity ($c_q$) dependent (nonlinear) diffusion for each internal waves. In addition, we compare with a monotony preserving (MP) scheme which is known to perform better around smooth extrema ([4, 18]. The results in figure (9) show that this effectively damps the computational mode, as confirmed by the plot of the corresponding RMS error in figure (10). Note also the much better behavior of the MP scheme against the TVD scheme. Even if a little of dispersion is visible for high baroclinic modes, the 2km fourth order MP solution is closed to the analytical solution. Unlike all other schemes introduced so far, it leads to a non-oscillatory scheme for the propagation of internal gravity waves.

# 5 Direct space time algorithms

Even if seldom implemented in ocean models, direct space time algorithms are sometimes used to discretize momentum advection terms (e.g. [1]). The advantages of this approach are well

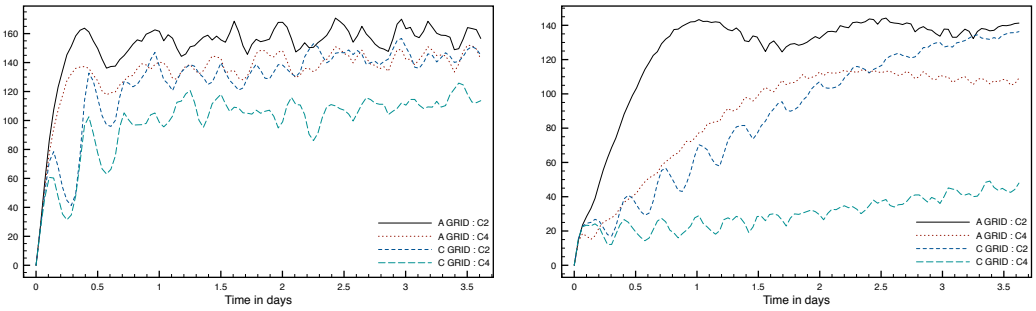


Figure 8: Relative RMS error (in %) for $\Delta x = 4$km (left) and $\Delta x = 2$km (right)

known: it allows to construct high order schemes in space and time with minimal stencil through only one evaluation of the right hand side together with a stability condition which remains unity when the order is increased. For multidimensionnel problems, direct space time algorithms have direct extensions via a Multidimensional Advective-Conservative Hybrid Operator (MACHO) approach ([6]) or via a directional splitting approach ([2]). The computation of the eigenvalues of the normal mode decomposition allows the design of direct space time algorithms specifically designed for the internal waves propagation. The schemes derived in this section, both on staggered and nonstaggered grids, are basically constructed for a shallow water model, it can therefore be used in several different contexts. The objective is to build direct space time schemes for the following system of equations

$$\begin{aligned} \frac{\partial u}{\partial t} + g\frac{\partial h}{\partial x} &= 0 \\ \frac{\partial h}{\partial t} + \frac{c^2}{g}\frac{\partial u}{\partial x} &= 0 \end{aligned} \tag{18}$$

## 5.1 Non Staggered grid formulation

The formulation of space time algorithms in the scalar case is well known and can be directly extended to system (18) when the grid is not staggered. On the non staggered grid, the resulting scheme can either be formulated in terms of characteristic (as in (13)) or primitive variables (as in (18)) since there is no ambiguity in the discrete definition of the characteristic variables. We chose to formulate the scheme in term of primitive variables so that the extension to the non staggered grid will follow the same ideas. The time evolution of $u_i$ and $h_i$ is written as

$$\begin{aligned} u_i^{n+1} &= u_i^n - g\frac{\Delta t}{\Delta x}\left(F^u_{i+1/2} - F^u_{i-1/2}\right) + G^u_{i+1/2} - G^u_{i-1/2} \\ h_i^{n+1} &= h_i^n - \frac{c^2}{g}\frac{\Delta t}{\Delta x}\left(F^h_{i+1/2} - F^h_{i-1/2}\right) + G^h_{i+1/2} - G^h_{i-1/2} \end{aligned}$$

where the interfacial fluxes are given by:

$$\begin{aligned} F^u_{i+1/2} &= \alpha_{i-1}h^n_{i-1} + \alpha_i h^n_i + \alpha_{i+1}h^n_{i+1} + \alpha_{i+2}h^n_{i+2} \\ G^u_{i+1/2} &= \beta_{i-1}u^n_{i-1} + \beta_i u^n_i + \beta_{i+1}u^n_{i+1} + \beta_{i+2}u^n_{i+2} \end{aligned} \tag{19}$$

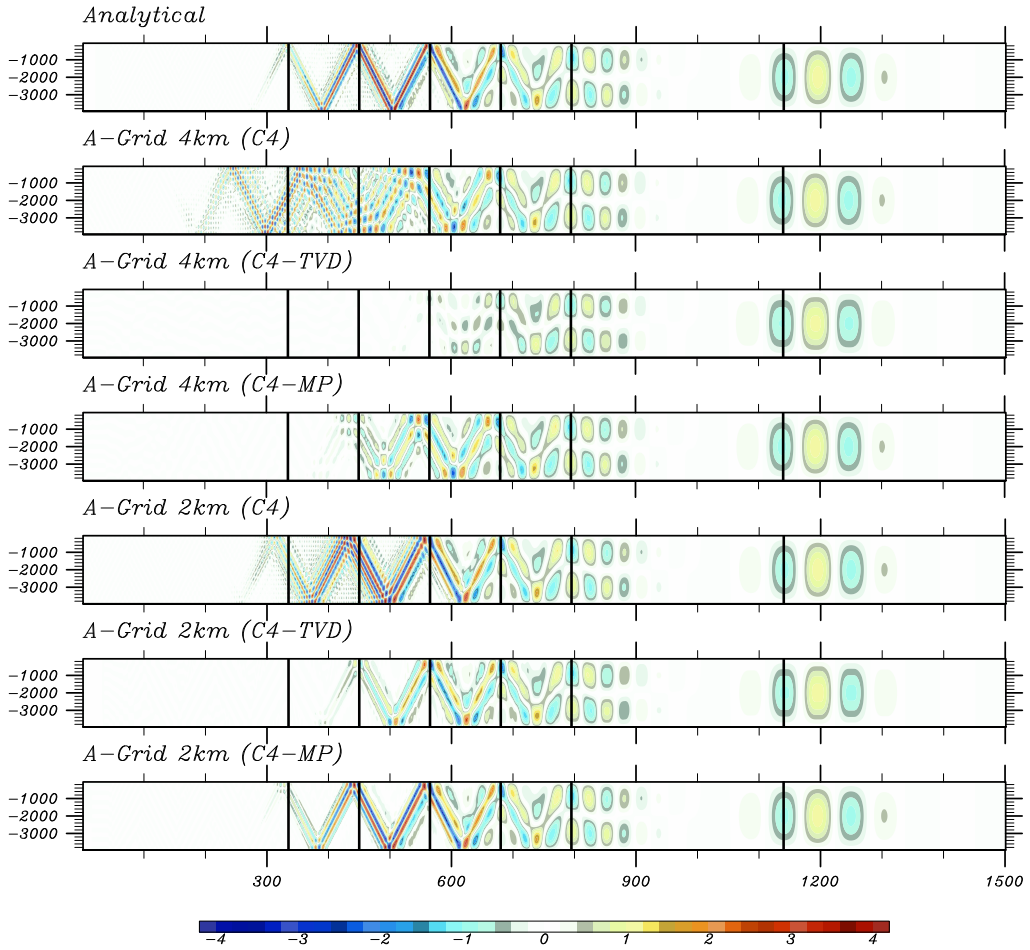


Figure 9: Numerical solutions on the A-GRID. Results at 4 and 2km with the fourth order centered scheme (C4) and with added TVD (C4-TVD) or MP limiters (C4-MP)

Exchanging $u$ and $h$ in (19) leads to the expressions of $F^h_{i+1/2}, G^h_{i+1/2}$. Fourier transform and Taylor expansion at large scales shows that second order in space and time is achieved by setting

$$\alpha_{i-1} = \alpha_{i+2} = 0,\ \alpha_i = \alpha_{i+1} = \frac{1}{2}, \quad \beta_{i-1} = \beta_{i+2} = 0,\ \beta_i = -\frac{\mu^2}{2}, \beta_{i+1} = -\beta_i$$

where $\mu = c\dfrac{\Delta t}{\Delta x}$ is the Courant number. For this particular choice of the $\alpha$ and $\beta$ weights, the resulting scheme is equivalent to a Lax Wendroff scheme on the characteristic variables.
Fourth order space time accuracy is achieved by setting

$$\alpha_{i-1} = \alpha_{i+2} = -\frac{1}{12} + \frac{\mu^2}{12},\ \alpha_i = \alpha_{i+1} = \frac{7}{12} - \frac{\mu^2}{12}$$
$$\beta_{i-1} = \frac{1}{24}\mu^2(1-\mu^2), \beta_{i+2} = -\beta_{i-1},\ \beta_i = \frac{1}{8}\mu^2(-5+\mu^2), \beta_{i+1} = -\beta_i$$

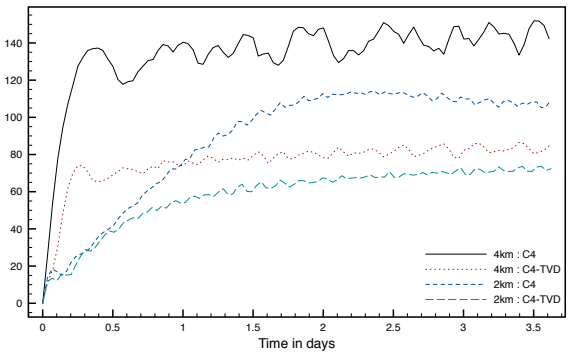


Figure 10: Relative RMS error with fourth order centered (C4) and fourth order TVD (C4-TVD) schemes on a $A$-grid

For the first order hyperbolic shallow-water system (18), the obtained coefficients simply translates the fact that the even order temporal derivates of $u$ (resp. $h$) is replaced by even order spatial derivatives of $u$ (resp. $h$) and that odd order temporal derivates of $u$ (resp. $h$) is replaced by odd order spatial derivatives of $h$ (resp. $u$). As for other direct space time algorithms, both second and fourth order schemes are exact for $\mu = \pm 1$.

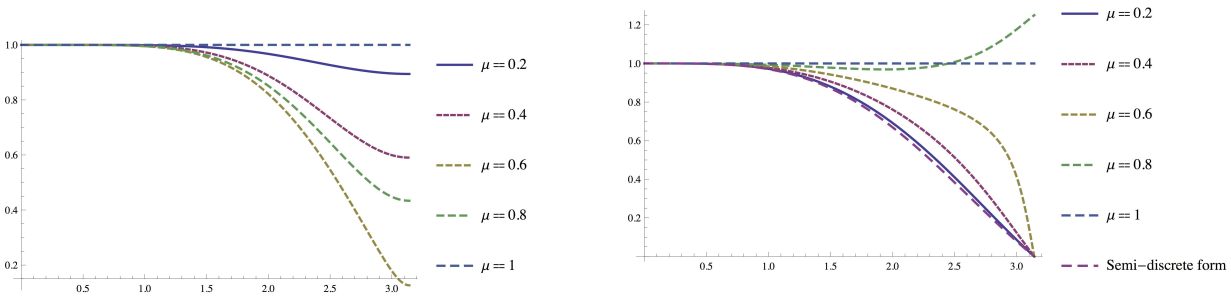


Figure 11: Dissipation error (left) and dispersion error (right) with respect to the wavenumber $k\Delta x$ for the fourth order direct space time algorithm on a $A$-grid for different values of the Courant number $\mu$.

## 5.2 Staggered grid formulation

For the staggered grid formulation, we start from a similar expression on a staggered grid: ($h$ is located at $i + 1/2$ points, see figure (3)):

$$u_i^{n+1} = u_i^n - g\frac{\Delta t}{\Delta x}\left(F^u_{i+1/2} - F^u_{i-1/2}\right) + G^u_{i+1/2} - G^u_{i-1/2}$$

$$h^{n+1}_{i+1/2} = h^n_{i+1/2} - \frac{c^2}{g}\frac{\Delta t}{\Delta x}\left(F^h_{i+1} - F^h_{i-1}\right) + G^h_{i+1} - G^h_i$$

where

$$\begin{aligned} F^u_{i+1/2} &= \alpha_{i-3/2}h^n_{i-3/2} + \alpha_{i-1/2}h^n_{i-1/2} + \alpha_{i+1/2}h^n_{i+1/2} + \alpha_{i+3/2}h^n_{i+3/2} + \alpha_{i+5/2}h^n_{i+5/2} \\ G^u_{i+1/2} &= \beta_{i-1}u^n_{i-1} + \beta_i u^n_i + \beta_{i+1}u^n_{i+1} + \beta_{i+2}u^n_{i+2} \end{aligned} \tag{20}$$

$F^h_i$ and $G^h_i$ are obtained by interchanging $u$ and $h$ in (20) and by adding 1/2 to the indices. Second order in space and time is achieved by setting

$$\alpha_{i+5/2} = \alpha_{i-3/2} = 0, \alpha_{i-1/2} = \alpha_{i+3/2}, \alpha_{i+1/2} = 1 - 2\alpha_{i-1/2}$$
$$\beta_{i-1} = \beta_{i+2} = 0,\ \beta_i = -\frac{\mu^2}{2}, \beta_{i+1} = -\beta_i$$

Setting $\alpha_{i-1/2} = \alpha_{i+3/2} = 0$ leads to an unstable scheme (the module of the amplification factor is given at large scales by $|\lambda| = 1 + \mu^2\left(\frac{\mu^2}{8} - \alpha_{i+3/2}\right)$). Here we choose a value of $\alpha_{i-1/2}$ which leads to a stability condition of $|\mu| \leq 1$.

$$\alpha_{i-1/2} = \frac{1}{4}\left(1 - \sqrt{1-\mu^2}\right) \tag{21}$$

The details of the computation are not given but it consists in looking at the module of the amplification factor at large ($\theta = k\Delta x \ll 1$) and small scales ($\theta = k\Delta x = \pi$) and in finding the constraint such that it is less than one (and this can indeed be achieved only for $|\mu| \leq 1$ among all the choices for $\alpha_{i-1/2}$. $\alpha_{i-1/2}$ given by (21) thus leads to the largest stability limit of this family). Fourth order accuracy in space and time is obtained for

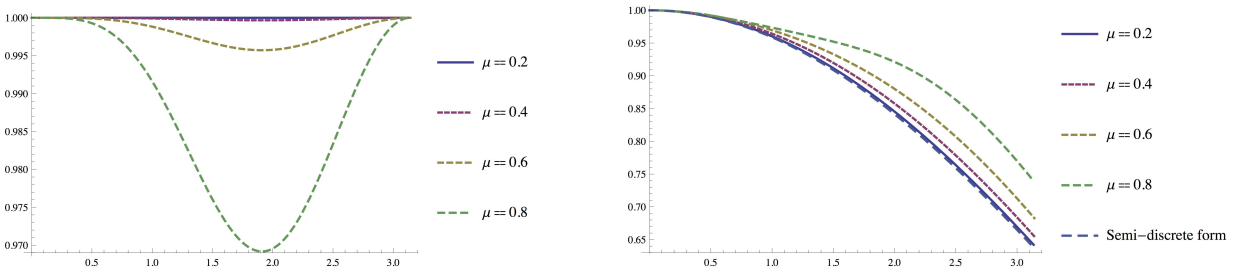


Figure 12: Same as figure 11 for the second order direct space time algorithm on a $C$-grid

$$\alpha_{i-1/2} = \alpha_{i+3/2} = -\frac{1}{24} + \frac{\mu^2}{6} - 4\alpha_{i-3/2}, \alpha_{i+1/2} = \frac{13}{12} - \frac{\mu^2}{3} + 6\alpha_{i-3/2}, \alpha_{i+5/2} = \alpha_{i-3/2}$$
$$\beta_{i-1} = \frac{1}{24}\mu^2(1-\mu^2), \beta_{i+2} = -\beta_{i-1},\ \beta_i = \frac{1}{8}\mu^2(-5+\mu^2), \beta_{i+1} = -\beta_i$$

Here trying to minimize the stencil by setting $\alpha_{i-3/2}$ to 0 also leads to an unstable scheme. The choice that leads to a stability condition of $|\mu| \leq 1$ is

$$\alpha_{i-3/2} = \min\left(\frac{1}{96}\left(4\mu^2 - 7\right) + \frac{1}{48}\sqrt{-\mu^6 + 8\mu^4 - 19\mu^2 + 12}, \frac{8\mu^4 - 16\mu^2 - 1}{1152}\right)$$

Again this choice of $\alpha_{i-3/2}$ comes from a study of module of the amplification factor at large (second term in the minimum above) and small scales (first term in the minimum above).

### 5.3 Analysis

Space time dispersion errors are plotted on figure (11). In particular, it can be shown that for the $A$-grid the numerical mode is removed for $1 \geq |\mu| \geq \sqrt{\frac{1}{2}\left(4-\sqrt{10}\right)} \approx 0.65$.

Unlike the nonstaggered case, the direct space time schemes are not exact for $\mu = 1$ on the staggered grid[4]. But the CFL stability condition is still one. This leads to a very efficient algorithm. The stability limit of these schemes can still be increased by using classical forward backward approaches. The results obtained with these direct space time schemes (not shown) are almost identical to the ones obtained with the separated space time approach (i.e. RK4-C2 or RK4-C4) both for staggered and nonstaggered grids, but again with a far better efficiency. In the case of the $A$-grid, TVD or monotonicity preserving direct space time schemes can easily be derived.

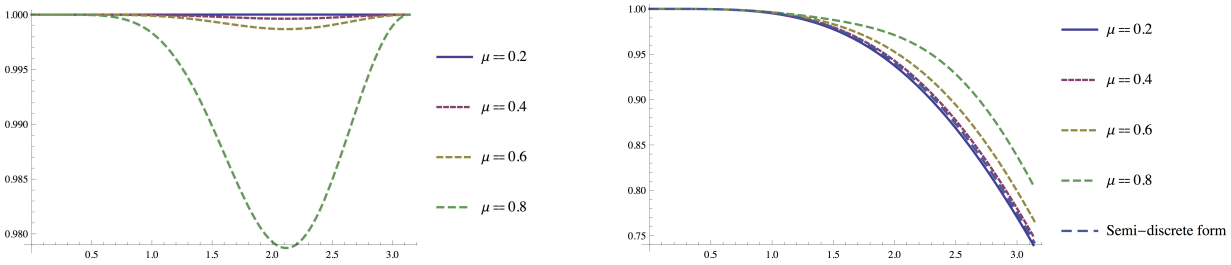


Figure 13: Same as figure 11 for the fourth order direct space time algorithm on a $C$-grid

## 6 Conclusion and perspectives

The numerical approximation of internal waves propagation has been studied in this paper. We, first, emphasized the fact that the use of high order approximations allow much better discrete dispersion relation, even for staggered grids. In addition to the use of high order pressure gradient computation, it requires a high order computation of the horizontal divergence term in the continuity equation. Thanks to an explicit computation of internal gravity waves phase speeds, we introduced an efficient flow-dependent damping term to dissipate the non resolved modes, which is important when using non staggered grids. We also derived direct space-time algorithms that show great efficiency both in terms of stability and accuracy. Those schemes can be easily extended to satisfy monotonicity constraints for internal wave propagation on non staggered grid, however the design of such monotonic schemes remains challenging on staggered grids. The study of internal wave breaking, acting like hydraulic jumps, could probably benefit from the use of such schemes.

## Acknowledgements

E. Blayo, J. Demange, L. Debreu, and P. Marchesiello were funded by the ANR through contract ANR-11-MONU-005 (COMODO). F. Lemarié acknowledges the support of the French LEFE MANU and GMMC programs through project CHRONOS.

[4]This essentially comes from the fact that the Euler time scheme has an error that expands in term of $\Delta t$ while the spatial derivatives have an error that expands in term of $\Delta x/2$ instead of $\Delta x$ on a non staggered grid.

# References

[1] Adcroft A., J.-M. Campin, S. Dutkiewicz, C. Evangelinos, D. Ferreira, G. Forget, B. Fox-Kemper, P. Heimbach, C. Hill, E. Hill, H. Hill, O. Jahn, M. Losch, J. Marshall, G. Maze, D. Menemenlis, and A. Molod. MITGCM USER MANUAL. In MIT Department of EAPS 77 Massachusetts Ave. Cambridge, MA 02139-4307. March 10, 2014, 2014. 470 pp.

[2] Bott A. Improving the time-splitting errors of one-dimensional advection schemes in multi-dimensional applications. Atmospheric Research, 2010.

[3] Brown J. A. and K. A. Campana. An economical time-differencing system for numerical weather prediction. Mon. Weather Rev., 106:1125–1136, 1978.

[4] Suresh A. and H.T. Huynh. Accurate monotonicity-preserving schemes with runge-kutta time stepping. J. Comput. Physics, 136(1):83 – 99, 1997.

[5] Cushman Roisin B. and J. M. Beckers. Introduction to Geophysical Fluid Dynamics: Physical and Numerical Aspects. Academic Press, 2010.

[6] Leonard B.P., A.P. Lock, and M.K. MacVean. Conservative explicit unrestricted time step multidimensional constancy preserving advection schemes. Mon. Weather Rev., 124:2588–2606, May 1996.

[7] Griffiths S. D. and R. H. J. Grimshaw. Internal tide generation at the continental shelf modeled using a modal decomposition: Two-dimensional results. J. Phys. Oceanogr., 37(3):428–451, 2014/08/28 2007.

[8] Blayo E. and L. Debreu. Revisiting open boundary conditions from the point of view of characteristic variables. Ocean Modell., 9(3):231 – 252, 2005.

[9] Gouillon F. Internal wave propagation and numerically induced diapycnal mixing in oceanic general circulation models. PhD thesis, Florida state university - College of arts and sciences, 2010.

[10] Shchepetkin A. F. and J. C. McWilliams. The regional oceanic modeling system (roms): a split-explicit, free-surface, topography-following-coordinate oceanic model. Ocean Modell., 9(4):347 – 404, 2005.

[11] Demange J., L. Debreu, P. Marchesiello, F. Lemarié, and E. Blayo. Depth-dependent barotropic integration and stability through vertical modes in free-surface ocean models. Ocean Modell., 2014. under review.

[12] Dukowicz J. K. Mesh effects for rossby waves. J. Comput. Physics, 119(1):188 – 194, 1995.

[13] Kundu P. K. and Cohen I. M. Fluid Mechanics, Second Edition. Academic Press, 2002.

[14] Beckers J. M. Selection of a staggered grid for inertia-gravity waves in shallow water. International Journal for Numerical Methods in Fluids, 38(8):729–746, 2002.

[15] Griffies S. M., C. Boning, F. O. Bryan, E. P. Chassignet, R. Gerdes, H. Hasumi, A. Hirst, A.-M. Treguier, and D. Webb. Developments in ocean climate modelling. Ocean Modell., 2:123–192, 2000.

[16] Durran D. R. Numerical Methods for Fluid Dynamics : With Application to Geophysics. Springer Press, 2010.

[17] Osborn T. R. Estimates of the local rate of vertical diffusion from dissipation measurements. J. Phys. Oceanogr., 10(1):83–89, 1980.

[18] Daru V. and C. Tenaud. High order one-step monotonicity-preserving schemes for unsteady compressible flow calculations. J. Comput. Physics, 193:563–594, 2004.

[19] Le Roux D. Y. Spurious inertial oscillations in shallow-water models. J. Comput. Physics, 231(24):7959–7987, 2012.

# Contents

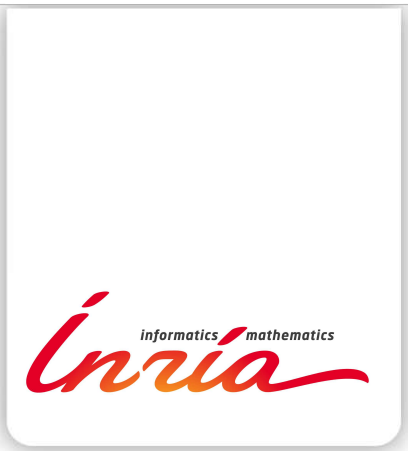


**RESEARCH CENTRE**
**GRENOBLE – RHÔNE-ALPES**

Inovallée
655 avenue de l'Europe Montbonnot
38334 Saint Ismier Cedex

Publisher
Inria
Domaine de Voluceau - Rocquencourt
BP 105 - 78153 Le Chesnay Cedex
inria.fr

ISSN 0249-6399